J Fluoresc (2014) 24:1811–1825
DOI 10.1007/s10895-014-1470-4

ORIGINAL PAPER

Novel Twisted Intramolecular Charge Transfer (TICT) Extended Fluorescent Styryl Derivatives Containing Quinoline Electron Releasing Moiety

Mininath S. Deshmukh · Nagaiyan Sekar

Received: 9 July 2014 / Accepted: 29 September 2014 / Published online: 14 October 2014

Abstract Novel extended fluorescent styryl derivatives were synthesized from (E)-3-(2-cyclopropyl-4-(4-fluorophenyl)quinolin-3-yl)acrylaldehyde containing quinoline ring with 4-fluorophenyl ring at the 4-position as an electron donor and different active methylene compounds as electron acceptors by conventional Knoevenagel condensation reaction. The UV-Visible absorption and fluorescence emission spectra of the dyes were studied in solvents of differing polarity and the compounds showed polarity sensitive emission properties. The dyes were characterized by the spectral analysis. Thermogravimetric analysis showed these dyes are thermally stable up to 250 °C. Density Functional Theory computations have been used to derive more understanding of structural, molecular, electronic and photophysical parameters of the push-pull dyes. The computed absorption wavelength values are found to be in good agreement with the experimental results. The second order hyperpolarizability (β_o) values were computed by Density Functional Theory and found to be in the range of 116.61×10^{-31} to 898.48×10^{-31} e.s.u.

Keywords Quinoline · Extended styryl dyes · Hyperpolarizability · Solvatochromism · Thermally stable dyes · Photo-physics

Electronic supplementary material The online version of this article (doi:10.1007/s10895-014-1470-4) contains supplementary material, which is available to authorized users.

M. S. Deshmukh · N. Sekar (✉)
Tinctorial Chemistry Group, Institute of Chemical Technology (Formerly UDCT), N. P. Marg, Matunga, Mumbai 400 019, Maharashtra, India
e-mail: n.sekar@ictmumbai.edu.in

N. Sekar
e-mail: nethi.sekar@gmail.com

Introduction

Organic fluorescent heterocyclic chromophores have a wide range of applications in molecular probes[1], fluorescent markers[2], organic light-emitting diodes (OLED)[3], photovoltaic cells [4] and in traditional textile and polymer fields [5]. Electron donors like triphenylamine [6], diphenylamine [7] and carbazoles [8] with high electron mobility, thermal and photochemical stability are commonly used as hole-transporting materials or light-emitting materials for balanced charge injection find their importance in the above mentioned applications.

Quinoline unit occur in many fluorescent colorants with high quantum yield and have attracted much attention owing to their potential high technology applications [9, 10] including fluorescent probes in chemosensors [11], probes for DNA [12], zinc detection [13], and Hg^{2+} ion (water) detection [14]. Quinoline systems are well known substances with great therapeutic importance with respect to infectious diseases, particularly in the treatment of bacterial [15] and viral [16] infections. Also the cyclopropane ring is a main structural part in many synthetic and natural compounds that exhibits a wide range of biological activities from enzyme inhibition to antibiotic, herbicidal, antitumor, and HIV antiviral activities as non-nucleoside reverse transcriptase inhibitors [17–24].

A typical push– pull chromophore consists of a polar D-π-A system with a planar π-system end-capped by a strong electron donor (D) and a strong electron acceptor (A). The π-conjugated system ensuring intramolecular charge transfer (ICT) between the donor and the acceptor (A=−CN, −COOEt group etc.) is the most common of the conjugated double or triple bonds in aromatic and heteroaromatic rings as well as their combinations [25, 26]. There has always been an effort to design and synthesize novel, well-defined organic push-pull system with prospective applications as chromophores for nonlinear optics (NLO), electronic and photonic devices,

organic light-emitting diodes (OLED) and functional polymers 27].

In this paper, we have designed and synthesized a novel extended fluorescent styryl derivatives containing quinoline ring with 4-fluorophenyl ring at the 4-position as an electron releasing moiety and cyano or ester as an electron acceptor group. Generally the quinoline moiety acts as a mild electron withdrawing unit. But in the case of dyes synthesized here, the quinoline moiety acts as a mild donor due to presence of strong electron withdrawing cyano and carbethoxy groups in the extended styryl residue [28].

The ground and excited state geometries were optimized using density functional theory (DFT) with B3LYP functional combined with a 6-31G(d) basis set. Earlier studies have proposed that the twisting ICT model is able to explain the low frequency, strongly solvent-dependent energy band present in the fluorescence spectra as compared to, wagging, and planar intramolecular charge transfer (ICT) [29]. According to this model, the 8e molecule is calculated to be non-dual fluorescent in agreement with the experimental spectra. The single band observed in the fluorescence spectra of the dyes 8a–8f is due to a large stabilization of the charge-transfer excited state along the twisting coordinate. Also, the static first hyperpolarizability (β_o) and its related properties were calculated on the basis of the finite field approach [30]. The structures of the dyes synthesized are confirmed by using FT-IR, ^{1}H NMR and Mass spectral analysis. Also, their thermal stability and UV–vis absorption and fluorescence emission characteristics were studied.

Experimental

Materials and Equipment's

All the commercial reagents and solvents were procured from Sigma aldrich and were used without further purification. The reactions were monitored by TLC using on 0.25 mm E-Merck silica gel 60 F_{254} precoated plates, which were visualized with UV light. Melting points were measured on standard melting point apparatus from Sunder industrial product Mumbai, and are uncorrected. The FT-IR spectra were recorded on Perkin Elmer 257 spectrometer using KBr discs. ^{1}H-NMR spectra were recorded on VARIAN 400-MHz instrument (USA) using TMS as an internal standard. Mass spectra were recorded on Finnigan mass spectrometer. The visible absorption spectra of the compounds were recorded on a Spectronic Genesys 2 UV-Visible spectrometer, fluorescence emission spectra were recorded on Varian Cary Eclipse fluorescence spectrophotometer using freshly prepared solutions at the concentration 1×10^{-6} mol L^{-1} solution. Simultaneous DSC-TGA measurements were performed out on SDT Q 600 v8.2 Build 100 model of TA instruments Waters (India) Pvt. Ltd.

Fluorescence quantum yields were determined in different solvents by using quinine sulfate (0.54 in ethanol) [31] as a reference standard using the comparative method.

Computational Methods

All the computations were performed using the Gaussian 09 package [32]. The ground state (S0) geometry of the synthesized styryl dyes in their C1 symmetry was optimized in the gas phase using Density Functional Theory (DFT) [33]. The functional used was B3LYP. The B3LYP method combines Becke's three parameter exchange functional (B3) [34] with the nonlocal correlation functional by Lee, Yang and Parr (LYP) [35]. The basis set used for all the atoms was 6-31G(d). The same method was used for the vibrational analysis to verify that the optimized structures correspond to the local minima on the energy surface. The vibrational frequencies of the optimized structures were computed using the same method to verify that the optimized structures correspond to the local minima on the energy surface.

The vertical excitation energy and oscillator strengths at the ground state equilibrium geometries were calculated by using TD-DFT at the same hybrid functional and the basis set [36, 37]. The low-lying first singlet excited states (S1) of the dyes was relaxed using TD-DFT to obtain its minimum energy geometry. The difference between the energies of the optimized geometries at the first singlet excited state and the ground state was used to calculate the emission [38, 39]. The frequency computations were also carried out on the optimized geometry of the first excited singlet state of the dyes. All the computations in solvents of different polarities were carried out using the Self-Consistent Reaction Field (SCRF) under the Polarizable Continuum Model (PCM) [40]. The vertical electronic excitation spectra, including wavelengths, oscillators strengths, and main configuration assignment, were systematically investigated using TD-DFT with PCM model on the basis of the optimized ground state structures.

Synthetic Strategy

Six novel fluorescent quinoline based push-pull D-π-A extended styryl dyes have been synthesized. The styryl dyes contain 4-fluorophenyl along with the quinoline ring as an electron donor and cyano or carbethoxy group as electron acceptors conjugated through a π-bridge. They were synthesized by the classical Knoevenagel condensation of 3-substituted aldehyde 7 with the active methylene compounds a-f as shown in Scheme 1. In the first step, the methyl 2-cyclopropyl-4-(4-fluorophenyl)quinoline-3-carboxylate 3 was synthesized from 2-amino-4-fluorobenzophenone 1 and methyl cyclopropanecarbonylacetate 2. The compound 3 on reduction using DIBAL-H to give 4, which on mild oxidation using PCC offered the intermediate 5. The intermediate 5 was

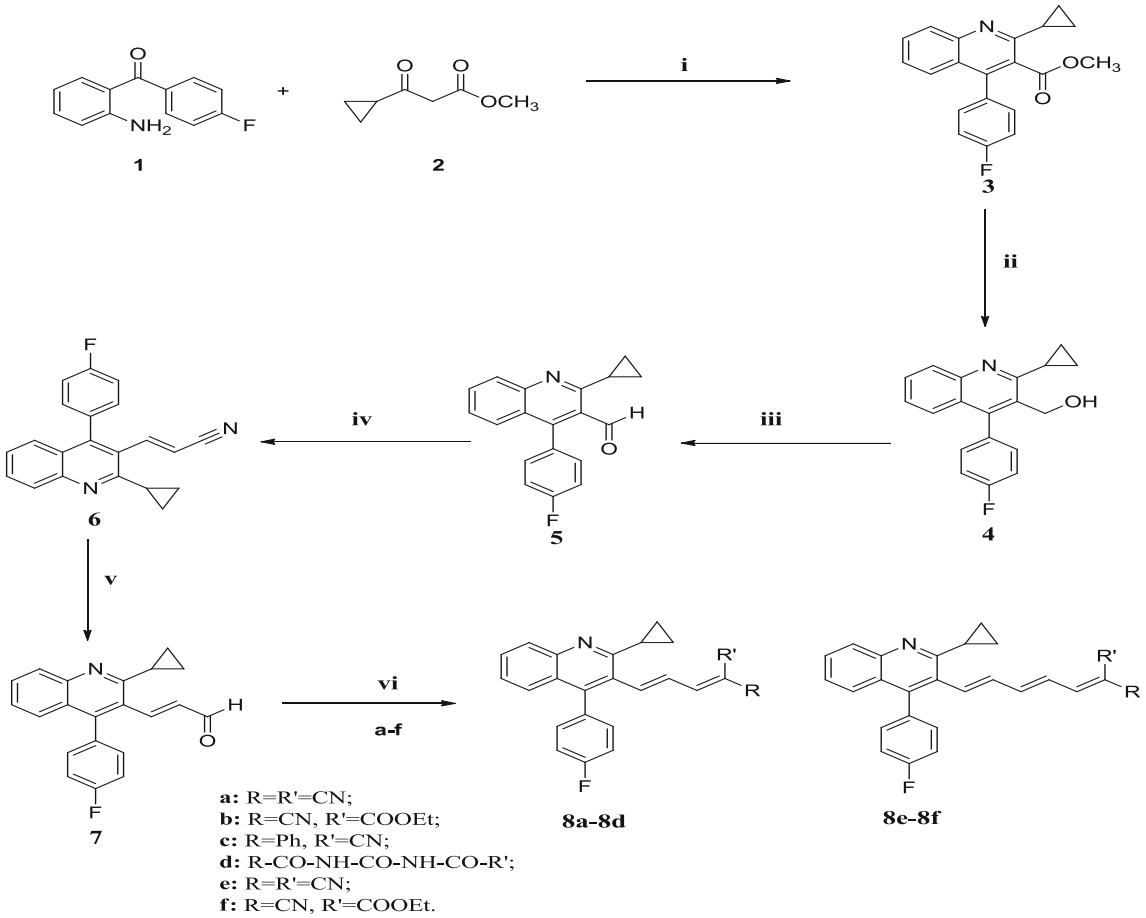

Scheme 1 Synthesis of styryl quinoline derivatives 8a–8f Reaction Condition: (i) H_2SO_4, AcOH, Reflux; (ii) DIBAL-H, Toluene, 25 °C; (iii) PCC, AcONa, CH_2Cl_2,25 °C; (iv) $(EtO)_2POCH_2CN$, NaOH(aq), $(n\text{-}C_8H_{17})_3MeNCl$, toluene, 25 °C; (v) DIBAL-H, toluene, 10 °C; (vi) Pipiridine, Ethanol, 25 °C

condensed with diethyl (cyanomethyl) phosphonate in the presence of trioctylmethylammonium chloride in alkaline medium to give the intermediate 6. The aldehyde 7 was obtained by selective reduction of the nitrile 6 using DIBAL-H in toluene at low temperature. Finally the aldehyde 7 and suitable active methylene compounds a–f were stirred in absolute ethanol containing a catalytic amount of piperidine to yield the desired styryl quinoline 8a-8f. The structures of the styryl compounds and all the intermediates were confirmed by FT-IR, ^{1}H NMR and Mass spectral analysis.

The absorption and emission spectra were measured to examine their photophysical properties. The solvatochromism and solvatofluorism behaviors of the molecules were studied by measuring the electronic absorption and emission spectra in different solvents.

Synthesis and Characterization

The synthetic scheme for the preparation of the dyes 8a-8f is shown in Scheme 1. (E)-3-[2-Cyclopropyl-4-(4-fluorophenyl)-3-quinolinyl]-2-propenal (7) was prepared by the reported procedure [41, 42] from 2-amino-4-fluorobenzophenone (1) and methyl 3-cyclopropyl-3-oxopropanoate (2).

General Procedure of Synthesis of Styryl 8a-8f

A mixture of (E)-3-[2-cyclopropyl-4-(4-fluorophenyl)-3-quinolinyl]-2-propenal 7 (0.25 g, 0.7 mmol) active methylene (a–f) (0.7 mmol) and 1 drop of piperidine in 10 ml ethanol was stirred at room temperature for 8 h. The reaction was monitored by thin layer chromatography, after completion of the reaction, the product precipitated. The precipitated product was filtered and recrystalized from a small amount of ethanol to offer the pure 8a–8f.

(E)-2-(3-(2-Cyclopropyl-4-(4-fluorophenyl)-3-quinolinyl)-allylidene) malononitrile (8a):

Yield: 85 %. Colored: Yellow. Melting Point: 234–236 °C. IR (cm^{-1} KBr): 2215, 1690, 1584, 969.

^{1}HNMR (400 MHz, $CDCl_3$): 1.17 (m, 2H), 1.46 (m, 2H), 2.44 (m, 1H), 7.03 (d, 1H, J=14.8 Hz), 7.27 (m, 3H), 7.37 (m, 4H), 7.59 (m, 1H), 7.64 (m, 1H), 7.99 (d, 1H, J=8 Hz). FAB-MS m/z: 366.1 $[M+H]^+$.

(2E,4E)-Ethyl-2-cyano-5-(2-cyclopropyl-4-(4-fluorophenyl)quinolin-3-yl)penta-2,4-dienoate (8b):

Yield: 82 %. Colored: Yellow. Melting Point: 174–176 °C. IR (cm^{-1} KBr): 2207, 1709, 1692, 1585, 1230,

971. ^{1}HNMR (400 MHz, $CDCl_3$): 1.15 (m, 2H), 1.37 (t, 3H), 1.46 (m, 2H), 2.37 (m, 1H), 4.32 (q, 2H), 7.06 (dd, 1H, J= 11.6 and 16 Hz), 7.26 (m, 4H), 7.36 (d, 1H, J=16 Hz), 7.37 (m, 2H), 7.66 (m, 1H), 7.82 (d, 1H, J=11.6Hz), 7.99 (d, 1H, J=7.6 Hz). FAB-MS m/z: 413.3 $[M+H]^+$.

(2E,4E)-5-(2-cyclopropyl-4-(4-fluorophenyl)quinolin-3-yl)-2-phenylpenta-2,4-dienenitrile (8c):

Yield: 70 %. Colored: Faint Yellow. Melting Point: 166-168 °C. IR (cm^{-1} KBr): 2195, 1692, 1587, 969. ^{1}HNMR (400 MHz, $CDCl_3$): 1.15 (m, 2H), 1.46(m, 2H), 2.4 (m, 1H), 7.03 (d, 1H, J=14.8 Hz), 7.26 (m, 5H), 7.37 (m, 5H), 7.59 (m, 2H), 7.64 (m, 1H), 7.91 (d, 1H, *J* =8.4Hz). FAB-MS m/z: 417.2 $[M+H]^+$.

(E)-5-(3-(2-Cyclopropyl-4-(4-fluorophenyl)quinolin-3-yl)allylidene)pyrimidine-2,4,6(1H,3H,5H) trione (8d):

Yield: 90 %. Colored: Yellow. Melting Point: 280 °C decomposed. IR (cm^{-1} KBr): 3614, 1712, 1649, 1587, 970. ^{1}HNMR (400 MHz, $CDCl_3$): 1.17 (m, 2H), 1.48 (m, 2H), 2.43 (m, 1H), 7.24 (m, 4H), 7.39 (d, 4H, *J*=7.6Hz), 7.57 (d, 1H, *J*=16Hz), 7.68 (m, 1H), 7.97 (dd, 2H, *J*=8.4Hz and 12Hz), 8.17 (s, 1H), 8.29 (s, 1H), 8.44 (m, 1H). FAB-MS m/z: 428.3 $[M+H]^+$.

2-((2E,4E)-5-(2-Cyclopropyl-4-(4-fluorophenyl)quinolin-3-yl)-1-phenylpenta-2,4-dien-1-ylidene)malononitrile (8e):

Yield: 75 %. Colored: Yellow. Melting Point: 220–221 °C. IR (cm^{-1} KBr): 2218, 1691, 1580, 970. ^{1}HNMR (400 MHz, $CDCl_3$): 1.08 (m, 2H), 1.41 (m, 2H), 2.32 (m, 1H), 6.5 (dd, 1H, *J*=10.8 and 14.4 Hz), 6.68 (dd, 1H, *J*=10.8 and 15.6 Hz), 6.88 (d, 1H, *J*=15.6), 6.96 (d, 1H, *J*=14.4 Hz), 7.32 (m, 4H), 7.41 (m, 4H), 7.55 (m, 3H), 7.65 (m, 1H), 7.96 (d, 1H, *J*=8.4 Hz). FAB-MS m/z: 467.1 $[M]^+$.

(2E,4E,6E)-Ethyl 2-cyano-7-(2-cyclopropyl-4-(4-fluorophenyl)quinolin-3-yl)-3-phenylhepta-2,4,6-trienoate (8f):

Yield: 68 %. Colored: Yellow. Melting Point: 192–194 °C. IR (cm^{-1} KBr): 2220, 1708, 1683, 1583, 1235, 970. ^{1}HNMR (400 MHz, $CDCl_3$): 1.08 (m, 2H), 1.35 (t, 3H), 1.41 (m, 2H), 2.40 (m, 1H), 4.29 (q, 2H), 6.38 (d, 2H, J=15.2), 6.63 (m, 4H), 6.77 (d, 2H, J=15.6 Hz), 7.21 (m, 3H), 7.33 (m, 3H), 7.62 (m, 2H), 7.96 (d, 1H, J=8.4 Hz). FAB-MS m/z: 533.3 $[M+H_2O]^+$.

Results and Discussion

Photo-physical Properties

To evaluate the effect of the solvent polarities on the photophysical properties of the extended styryl derivatives (8a–8f), absorption and emission studies were carried out in eight different solvents of differing polarity, dielectric constant, refractive indices and the results obtained are summarized in Tables 4, 5, 6, 7, 8 amd 9, Figures S1-S5. The absorption maxima of the styryl dyes were found to be nearly same in all the solvents studied. From this it was clear that, the absorption properties of these dyes are independent of the solvent polarity.

The red shifted absorption maxima indicates that the dicyanovinyl moiety present in 8e (409 nm) has a stronger electron withdrawing effect than the cyano carbethoxy vinyl unit present in 8f (385 nm). This increases the charge transfer between the donors and acceptors. In the case of dyes 8a (352 nm) and 8b (373 nm) such a relation was not pronounced. The presence of extra double bond results in to the red shift in dyes 8e and 8f compared to 8a and 8d. As a result of this red shift, the band gap energy of the molecule gets decreased (Fig. 1).

During the emission study, it was found that the emissions of the compounds 8a–8f are affected by a change in the polarity and hydrogen bonding capacity of the solvents. These compounds with D-π-A structure consist of an electron-donating 4-fluorophenyl ring along with the quinoline moiety and an electron withdrawing cyano or carbethoxy group. The results showed that these compounds have pronounced solvatofluorism properties. The introduction of the electron accepting groups causes intramolecular charge transfer and mesomeric dipole moment. Depending on the electron affinity of the acceptor groups the CT band was blue or red shifted with a large Stokes shift. The dyes 8a, 8b, 8e and 8f showed a blue shift in the non-polar solvent (DCM) and a red shift in the polar solvent (DMF), while the dyes 8c and 8d showed a blue shift in the polar solvent (acetonitrile) and a red shift in the non-polar solvents (THF, acetone). The red shift observed in the polar solvent is indicative of the increased charge separation in the excited state, which results in a larger dipole moment than in the ground state [30]. The effect of solvent polarity on the absorption and emission behavior of the dye 8e is shown in Fig. 2.

Relative Quantum Yield

The fluorescence quantum yields of the synthesized styryl dyes were determined in different solvents and tabulated in Tables 4, 5, 6, 7, 8 and 9. The fluorescence quantum yields of the dyes mostly depend on both the nature of the substituent and the solvent polarity. Here, it has been observed that a decrease in the solvent polarity strongly enhances the fluorescence quantum yields of the styryl dyes 8a–8 f. The dyes showed higher quantum efficiencies in the non-polar solvents while lower quantum yields in the polar solvents. The highest quantum yield was observed in THF and the values in the increasing order are: 8e (0.02)<8c (0.06)<8b (0.07)<8d (0.11)=8f (0.11)<8a (0.12).

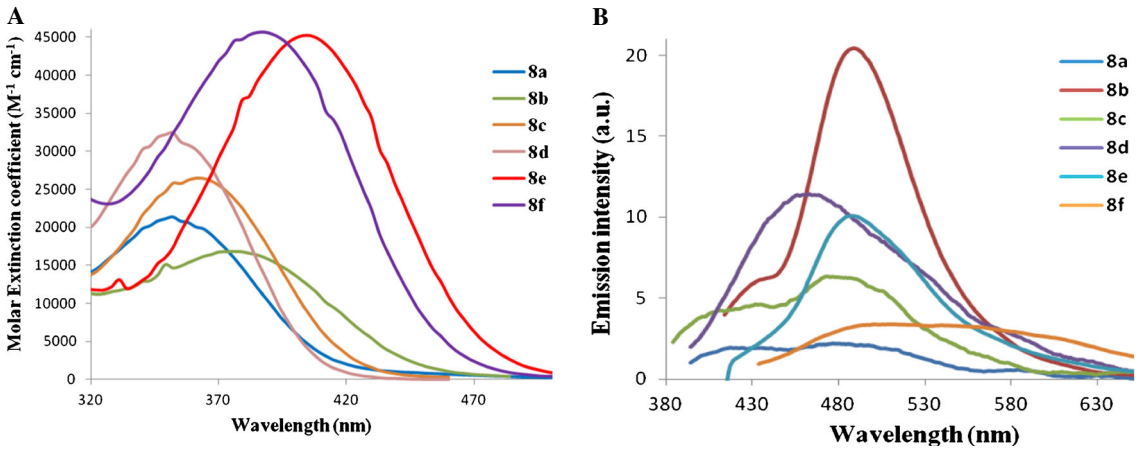

Fig. 1 **a** Absorption and **b** fluorescence spectra of dyes **8a–8f** in ethanol

Optimized Geometries of Dyes 8a–8f

The ground state geometries of the dyes were optimized at B3LYP/6-31G(d) level for the dyes 8a–8f. The optimized structures were having orthogonal arrangement of 4-fluorophenyl ring, cyclopropyl ring and twisting π-bridge acceptor cyano or carbethoxy group with quinoline moiety.

As a representative example, the structural view of the styryl dye 8f in the ground and the excited state is presented in Table 1, Fig. 3. In the dye 8f the major bond lengthening was observed between the bonds C_1-C_5, C_2-N_{38}, C_4-C_5, C_{24}-C_{26}, C_{27}-C_{65}, C_{40}-C_{41}, C_{42}-N_{43}, C_{55}-O_{56}, C_{55}-O_{57} by 0.020, 0.007, 0.035, 0.044, 0.040, 0.044, 0.004, 0.007, 0.012 Å and the bond length shortening for the bonds C_3-C_4, C_4-C_{14}, C_5-C_{24}, C_{26}-C_{27}, C_{65}-C_{40}, C_{40}-C_{44}, C_{41}-C_{42}, C_{41}-C_{55} by 0.013, 0.008, 0.045, 0.035, 0.031, 0.007, 0.013, 0.021 Å. Such a lengthening and shortening of the bonds were due to the effect of donor and acceptor groups present in the molecules. The excited state twist dihedral angle of the 4-fluorophenyl ring and the π -bridge contained acceptor cyano or carbethoxy at the terminal end with quinoline was reduced to maintain planarity. . Similar observations were observed in optimized geometry at ground and excited state of the remaining styryl dyes 8a–8e (Figures S6-S10).

Twisted Intramolecular Charge Transfer

In the instances of strong internal charge transfers in the ethylene chain of the donor-acceptor-substituted stilbenes and styryl dyes occuring upon excitation, there exist several possible routes of non radiative decay of the excitation energy [43]. These include the rotation around the central C=C bond, resulting in geometric isomerization, or rotation around one or two single bonds in the C-C=C-C fragment, leading to non emissive or weakly emissive a twisted intramolecular charge-transfer (TICT) excited state, which returns to the ground state without geometric isomerization [44].

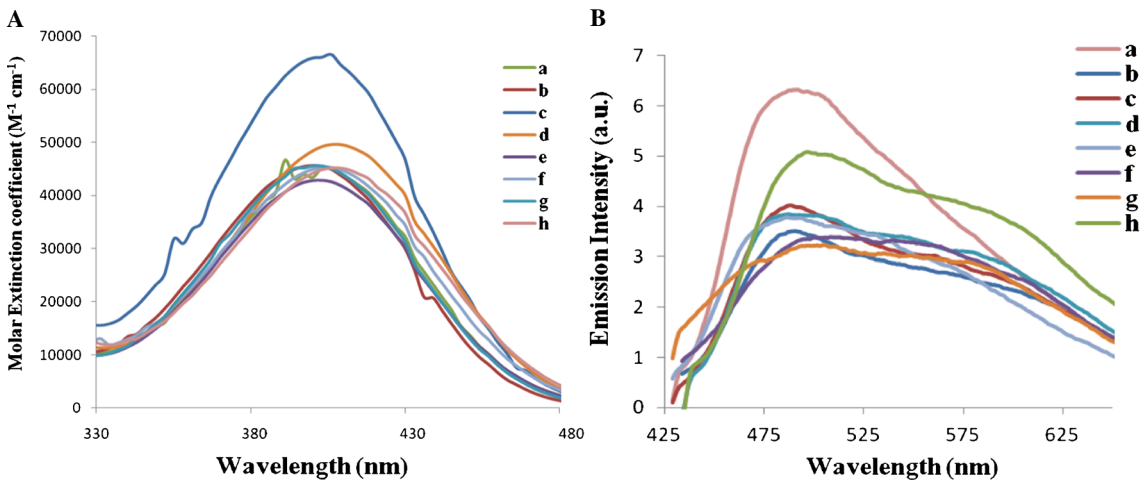

Fig. 2 **a** Absorption and **b** fluorescence spectra of dye **8e** in different solvent. Where, a = Tetrahydrofuran, b = Ethyl acetate, c = Acetone, d = Dichloromethane, e = Ethanol f = Methanol, g = Acetonitrile, h= N,N-Dimethylformamide

Table 1 Computed interatomic distances of dyes **8a–8f** in the ground state (GS) and excited state (ES) optimized geometry in DCM (Å)

Atom No	8a		8b		8c		8d		8e		8f	
	GS	ES	GS	ES	GS	ES	GS	ES	GS	ES	GS	ES
C1-C5	1.449	1.459	1.448	1.461	1.447	1.466	1.449	1.459	1.448	1.466	1.448	1.468
C4-C14	1.495	1.467	1.495	1.466	1.495	1.472	1.494	1.468	1.495	1.475	1.494	1.486
C4-C5	1.400	1.447	1.397	1.450	1.397	1.450	1.398	1.446	1.397	1.441	1.400	1.435
C5-C24	1.464	1.416	1.468	1.412	1.472	1.408	1.466	1.417	1.469	1.418	1.467	1.422
C21-F39	1.350	1.339	1.351	1.340	1.351	1.348	1.351	1.340	1.351	1.344	1.351	1.348
C24-C26	1.360	1.410	1.357	1.412	1.355	1.416	1.460	1.409	1.357	1.404	1.358	1.402
C26-C27	1.478	1.398	1.433	1.400	1.438	1.391	1.431	1.402	1.436	1.401	1.437	1.402
C27-C40	1.373	1.410	1.367	1.408	1.367	1.418	1.370	1.404	–	–	–	–
C27-C65	–	–	–	–	–	–	–	–	1.364	1.400	1.364	1.404
C40-C41	1.429	1.417	–	–	–	–	1.475	1.459	1.390	1.425	1.387	1.431
C65-C40	–	–	–	–	–	–	–	–	1.439	1.412	1.444	1.413

– Label bond atom is absent

The ground state optimized geometry of the dyes 8a–8f in DCM has a dihedral angle of 68–70° between the orthogonal 4-fluorophenyl and the quinoline segment C_5-C_4-C_{14}-C_{16}. The cyclopropyl ring is perpendicular and bends toward the quinoline nitrogen. In the dyes 8a, 8b, 8c there is also a small dihedral angle of 31.78°, 34.64°, 38.10° along C_4-C_5-C_{40}-N_{37} and in the dyes 8e-8f the angles 23.27–72.01° along C_4-C_5-C_{41}-N_{43} (the angle between the quinoline and the terminal cyano units respectively). The dihedral angle increases in the order: cyano < carbethoxy < phenyl group introduced at the terminal end. The pending phenyl ring on C_{40} atom of the π-bridge is twisted with a dihedral angle 57.01° and bends towards the quinoline moiety for dye 8e, while for the dye 8f 60.40° and nearly parallel to the 4-fluorophenyl ring present on the quinoline moiety.

In the excited state of the dyes 8a-8f, the orthogonal 4-fluorophenyl unit was twisted to a reduced dihedral angle between C_5-C_4-C_{14}-C_{16} up to 47°–62°. Similarly the terminal cyano, ester and the phenyl moiety are also twisted to a reduced dihedral angle amounting to reaching a planarity in the excited state (Table 2).

The Mulliken charge distribution in the ground and the excited state (DCM solvent) of the dyes 8a–8f are summarized

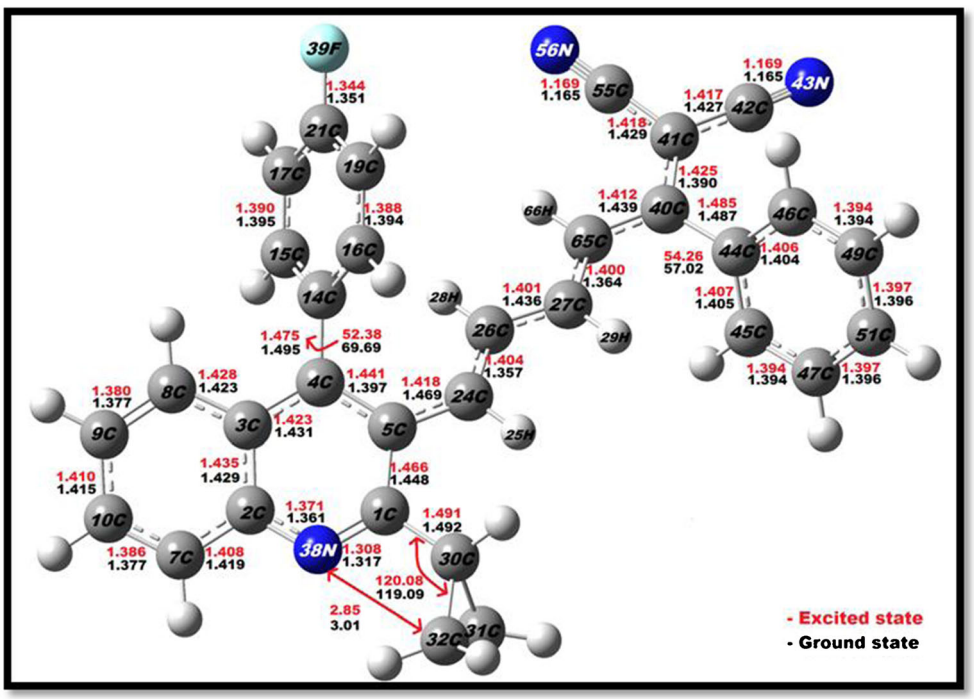

Fig. 3 Optimized geometry parameters of dye **8e** in DCM solvent in the ground state and excited state (bond lengths are in Å, dihedral angles are in degree °)

Table 2 Twist dihedral angle of dyes 8a-8f in the ground state (GS) and excited state (ES) optimized geometry in DCM

Styryl dyes	C_5-C_4-C_{14}-C_{16}		C_4-C_5-C_{40}-C_{37} /C_4-C_5-C_{41}-C_{53}		C_{65}-C_{40}-C_{44}-C_{46}	
	Ground state	Excited state	Ground state	Excited state	Ground state	Excited state
8a	70.91	47.98	31.78	29.07	–	–
8b	70.66	47.23	34.64	26.93	–	–
8c	70.29	49.14	38.10	26.93	–	–
8d	69.29	48.51	35.87	29.05	–	–
8e	69.69	52.38	24.78	05.41	57.01	54.26
8f	68.48	62.71	72.00	82.50	60.43	52.77

– Dihedral angle is absent

in Table 3, Figures S11-S16. In the excited state of the dye 8e, the net positive charge on the atom C_{21} and C_4 increases from 0.377 to 0.383 and 0.002 to 0.015. While the net negative charge on N atom increases from −0.529 to −0.541 (in au) (Fig. 4), which is suggestive of the charge delocalization in the molecule from the donor 4-fluorophenyl ring along with the quinoline unit to the dicyanovinyl acceptor moiety. The atom C_{40} (in dyes 8a, 8b, 8c and 8d) and in C_{41} (in dyes 8e and 8f) to which the cyano and carbonyl groups are attached possess a decreased net positive charge.

Electronic Vertical Excitations (TD-DFT)

The electronic vertical excitations were calculated using TD-B3LYP/6-31G(d) method. The experimental absorption wavelengths and the computed vertical excitation spectra associated with their oscillator strengths, composition, and their corresponding assignments of the dyes 8a–8f are summarized in Tables 4, 5, 6, 7, 8 and 9. The absorption band occurring at the lower energy with a higher oscillator strength is due to the intramolecular charge transfer (ICT) and it is the characteristic of the donor-π-acceptor push-pull dyes. These ICT bands for the dyes 8a, 8b, 8d and 8c, 8e, 8d were mainly due to the electronic transition from the highest occupied molecular orbital (HOMO-1) and HOMO to the lowest unoccupied molecular orbital (LUMO) respectively. The experimental absorption and the computed vertical excitation of the dyes 8a–8f are independent of the solvent polarity. The emission values were computed in three different solvents DCM, methanol and DMF. The computational fluorescence emission results

Table 3 Mulliken charge (e) distribution of dyes 8a–8f in the ground state (GS) and excited state (ES) optimized geometry in DCM

Atom No	8a		8b		8c		8d		8e		8f	
	GS	ES	GS	ES	GS	ES	GS	ES	GS	ES	GS	ES
C4	0.008	0.029	0.005	0.025	−0.004	0.006	0.007	0.028	0.002	0.015	−0.002	0.002
C5	0.063	0.049	0.060	0.048	0.062	0.050	0.061	0.049	0.061	0.055	0.061	0.083
C14	0.004	0.013	0.012	0.017	0.019	0.026	0.015	0.019	0.017	0.014	0.012	0.016
C21	0.380	0.385	0.379	0.385	0.378	0.382	0.379	0.383	0.377	0.383	0.379	0.381
C24	−0.210	−0.190	−0.213	−0.193	−0.230	−0.218	−0.212	−0.188	−0.226	−0.210	−0.219	−0.229
C26	−0.103	−0.125	−0.101	−0.125	−0.097	−0.109	−0.097	−0.124	−0.098	−0.111	−0.115	−0.129
C27	−0.078	−0.078	−0.109	−0.103	−0.148	−0.142	−0.168	−0.158	−0.096	−0.093	−0.100	−0.098
C36	0.308	0.290	0.288	0.280	0.265	0.253	–	–	–	–	–	–
N37	-0.519	-0.533	-0.536	-0.549	-0.547	-0.563	–	–	–	–	–	–
F39	-0.301	-0.290	-0.302	-0.291	-0.304	-0.298	-0.303	-0.292	-0.304	-0.294	-0.302	-0.299
C40	0.086	0.068	0.004	-0.012	0.065	0.055	-0.035	-0.043	0.156	0.159	0.092	0.110
N43	–	–	–	–	–	–	–	–	-0.526	-0.538	-0.541	-0.552
C44	–	–	–	–	-0.195	-0.201	–	–	0.020	0.032	0.015	0.036
C45	–	–	–	–	-0.188	-0.191	–	–	-0.162	-0.167	-0.158	-0.152
O48	–	–	–	–	–	–	-0.528	-0.545	–	–	–	–
C55	–	–	–	–	–	–	–	–	-0.305	-0.295	-0.149	-0.169
C65	–	–	–	–	–	–	–	–	-0.208	-0.226	-0.187	-0.196

– Label atom is absent

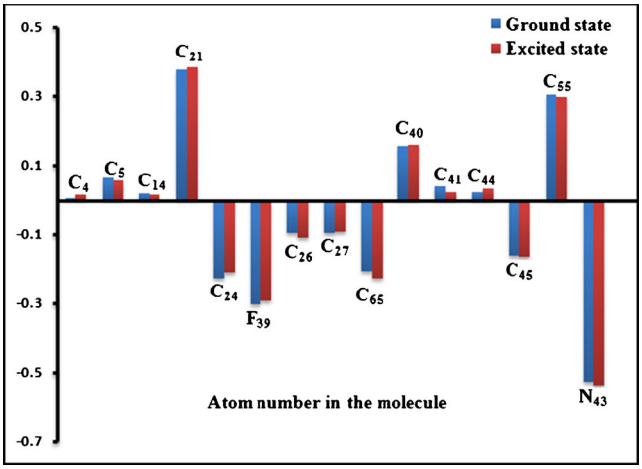

Fig. 4 Graph of Mulliken charge distribution on the dye **8e** in the ground and excited state optimized geometry in DMF

obtained by using TD-B3LYP/6-31G(d) were not able to reproduce the solvatofluorism behavior and the computations have shown almost nearly same value of the emission energy.

The dye 8a shows experimental absorption maxima in DCM (352 nm) and its computed vertical excitation transition energy difference between HOMO-1 to LUMO is 3.505 eV (353.63 nm) in DCM. There is a significant difference (~1.74 nm) and % deviation between the experimental absorption and the vertical excitation is in between 0.24 and 0.49 % in the studied solvents. Intense fluorescence emission peaks are observed in the non-polar solvents THF, and DCM compared to methanol, ethanol, DMF, DMSO. The difference between the experimental emission and the computed emission wavelengths in DCM (48 nm) and DMF (8 nm) are summarized in Table 4.

The dye 8b is fluorescent in solution and the computed vertical excitation value obtained from TD-DFT is in good agreement with the experimental absorption; the difference between the theoretical and the experimental values is less than 42 nm in all the solvents studied. The % deviation between the experimental absorption and the computed vertical excitation is between 9 and 11 % in the solvents studied. The difference between HOMO-1 to LUMO (82 %) transition is responsible for the vertical excitation located at 337.73 nm (3.671 eV) with an oscillator strength (f) 0.476. An intense fluorescence emission peak is observed in acetone and ethanol compared to the other solvents. The largest difference between the experimental emission and the computed emission wavelengths in DMF (8 nm) are summarized in Table 5.

In the case of dye 8c an intense emission peak was observed in THF, acetone and DMF. The experimental absorption maxima in DCM (361 nm) and the difference between the transition energy of HOMO to LUMO (95 %) is responsible for the vertical excitation located at 360.42 nm (3.44 eV) with an oscillator strength (f) 1.041. Theoretical vertical excitation values obtained from the TD-DFT computations is in good agreement with the experimental absorption. It was found that, the difference between the theoretical and the experimental values is less than 18 nm. The % deviation between the experimental absorption and the computed vertical excitation

Table 4 Observed UV-Visible absorption-emission and its computed vertical excitation spectra of absorption-emission of dye 8a in different solvents

Solvents	Experimental			Computed (TD-DFT)						Φ
	λ_{max}[a] nm ( )	λ_{max}[b] nm Intensity(au)	Stokes shift	Vertical[c] excitation (nm)	f[d]	Orbital contribution	%D[e]	TD-DFT emission (nm)	%D[f]	
THF	352 (30,259)	476 (38.82)	124	353.74	0.532	H-1→L (77%)	0.49	–	–	0.12
EtOAc	352 (19,710)	469 (10.97)	115	353.74	0.524	H-1→L (77%)	0.49	–	–	0.05
DCM	352 (19,564)	436 (28.11)	84	353.74	0.537	H-1→L (77%)	0.49	484	11.01	0.08
Acetone	352 (18,214)	488 (13.31)	136	353.63	0.526	H-1→L (77%)	0.46	–	–	0.04
EtOH	352 (21,389)	473 (06.32)	121	353.74	0.527	H-1→L (77%)	0.49	–	–	0.01
MeOH	352 (27,193)	470 (09.27)	55	352.83	0.520	H-1→L (77%)	0.24	490	3.21	0.02
ACN	352 (22,813)	479 (05.19)	127	353.63	0.524	H-1→L (77%)	0.46	–	–	0.01
DMF	352 (28,105)	483 (07.50)	131	353.63	0.542	H-1→L (77%)	0.46	491	0.23	0.01

[a] Experimental absorption wavelength

[b] Experimental emission wavelength

[c] Computed absorption wavelength

[d] Oscillator strength

[e] % Deviation between experimental absorption and vertical excitation computed by DFT

[f] % Deviation between experimental emission and computed (TD-DFT) emission

[Φ] Quantum yield at various solvents

–Not calculated

Table 5 Observed UV-Visible absorption-emission and its computed vertical excitation spectra of absorption-emission of dye 8b in different solvents

Solvents	Experimental			Computed (TD-DFT)						Φ
	λ_{max}[a] nm ( )	λ_{max}[b] nm intensity (au)	Stokes shift	Vertical[c] excitation (nm)	f[d]	Orbital contribution	%D[e]	TD-DFT emission (nm)	%D[f]	
THF	373 (19,034)	473 (08.29)	100	337.09	0.475	H-1→L (82%)	9.63	–	–	0.07
EtOAc	379 (31,312)	465 (03.73)	92	337.37	0.474	H-1→L (82%)	10.9	–	–	0.07
DCM	376 (19,199)	479 (05.53)	103	337.73	0.476	H-1→L (82%)	10.1	472	1.43	0.06
Acetone	373 (19,199)	480 (14.75)	107	338.19	0.477	H-1→L (82%)	9.33	–	–	0.07
EtOH	373 (16,810)	487 (20.46)	114	338.19	0.477	H-1→L (82%)	9.33	–	–	0.08
MeOH	373 (21,218)	484 (12.06)	111	338.29	0.477	H-1→L (82%)	9.31	478	1.24	0.05
ACN	373 (26,080)	481 (11.33)	108	338.29	0.477	H-1→L (82%)	9.31	–	–	0.04
DMF	373 (21,506)	487 (11.57)	114	338.29	0.478	H-1→L (85%)	9.31	479	1.64	0.03

[a] Experimental absorption wavelength

[b] Experimental emission wavelength

[c] Computed absorption wavelength

[d] Oscillator strength

[e] % Deviation between experimental absorption and vertical excitation computed by DFT

[f] % Deviation between experimental emission and computed (TD-DFT) emission

[Φ] Quantum yield at various solvents

– Not calculated

is between 0.1 and 2.4 % in the solvents studied. The difference between experimental and the computed emission wavelengths in DCM (46 nm) and methanol (14 nm) are summarized in Table 6.

Similarly to the dye 8a, the dye 8d the experimental absorption maxima in DCM (352 nm) and the transition between HOMO-1 to LUMO is responsible for the vertical excitation located at 353.84 nm (3.504 eV) with an oscillator strength

Table 6 Observed UV-Visible absorption-emission and its computed vertical excitation spectra of absorption-emission of dye 8c in different solvents

Solvents	Experimental			Computed (TD-DFT)						Φ
	λ_{max}[a] nm ( )	λ_{max}[b] nm Intensity (au)	Stokes shift	Vertical[c] excitation (nm)	f[d]	Orbital contribution	%D[e]	TD-DFT emission (nm)	%D[f]	
THF	361 (30,189)	475 (11.70)	114	360.05	1.035	H→L (95%)	0.26	–	–	0.06
EtOAc	361 (31,555)	445 (01.97)	84	360.21	1.024	H→L (95%)	0.22	–	–	0.01
DCM	361 (25,876)	447 (02.86)	86	360.42	1.041	H→L (95%)	0.16	493	10.29	0.02
Acetone	361 (28,054)	482 (05.63)	121	360.63	1.018	H→L (95%)	0.10	–	–	0.02
EtOH	367 (27,115)	477 (02.22)	110	360.63	1.019	H→L (95%)	1.74	–	–	0.01
MeOH	358 (32,580)	484 (04.57)	126	360.73	1.006	H→L (95%)	0.76	498	2.89	0.01
ACN	352 (40,693)	430 (02.81)	78	360.73	1.012	H→L (95%)	2.48	–	–	0.08
DMF	364 (38,003)	454 (18.88)	90	360.73	1.042	H→L (95%)	0.90	502	10.57	0.05

[a] Experimental absorption wavelength

[b] Experimental emission wavelength

[c] Computed absorption wavelength

[d] Oscillator strength

[e] % Deviation between experimental absorption and vertical excitation computed by DFT

[f] % Deviation between experimental emission and computed (TD-DFT) emission

[Φ] Quantum yield at various solvents

–Not calculated

Table 7 Observed UV-Visible absorption-emission and its computed vertical excitation spectra of absorption-emission of dye 8d in different solvents

Solvents	Experimental			Computed (TD-DFT)						Φ
	λ_{max}[a] nm ( )	λ_{max}[b] nm intensity (au)	Stokes shift	Vertical[c] excitation (nm)	f[d]	Orbital contribution	%D[e]	TD-DFT emission (nm)	%D[f]	
THF	352 (11,751)	467 (16.47)	115	353.67	0.487	H-1→L (87%)	0.66	–	–	0.11
EtOAc	352 (18,846)	468 (15.83)	116	353.74	0.491	H-1→L (87%)	0.69	–	–	0.09
DCM	352 (14,139)	458 (08.62)	106	353.84	0.493	H-1→L (90%)	0.73	492	7.42	0.05
Acetone	352 (10,072)	463 (07.80)	111	353.63	0.487	H-1→L (87%)	0.65	–	–	0.05
EtOH	352 (13,204)	463 (11.41)	111	353.74	0.487	H-1→L (87%)	0.69	–	–	0.08
MeOH	352 (11,283)	434 (11.74)	82	353.63	0.491	H-1→L (87%)	0.65	499	14.94	0.08
ACN	349 (11,491)	441 (05.20)	92	353.63	0.486	H-1→L (87%)	1.84	–	–	0.03
DMF	352 (11,041)	472 (08.73)	120	353.63	0.485	H-1→L (90%)	0.65	499	5.72	0.05

[a] Experimental absorption wavelength

[b] Experimental emission wavelength

[c] Computed absorption wavelength

[d] Oscillator strength

[e] % Deviation between experimental absorption and vertical excitation computed by DFT

[f] % Deviation between experimental emission and computed (TD-DFT) emission

[Φ] Quantum yield at various solvents

–Not calculated

(f) 0.491. There is a significant difference (~4 nm) and % deviation between the experimental absorption and the computed vertical excitation values which is between 0.65 and 1.84 % in the solvents studied. An intense fluorescence emission peak is observed in the non-polar solvent like THF and ethyl acetate. The % deviation between the experimental and the computed emission wavelengths in DCM (7.42) and DMF (4.45) are summarized in Table 7.

The dyes 8e and 8f experimental absorption maxima are 403 nm and 388 nm, while their computed vertical excitation

Table 8 Observed UV-Visible absorption-emission and its computed vertical excitation spectra of absorption-emission of dye 8e in different solvents

Solvents	Experimental			Computed (TD-DFT)						Φ
	λ_{max}[a] nm ( )	λ_{max}[b] nm intensity (au)	Stokes shift	Vertical[c] excitation (nm)	f[d]	Orbital contribution	%D[e]	TD-DFT emission (nm)	%D[f]	
THF	403 (45,252)	492 (06.31)	89	410.65	0.901	H→L (90%)	1.90	–	–	0.02
EtOAc	400 (45,673)	486 (03.78)	86	410.95	0.881	H→L (90%)	2.74	–	–	0.014
DCM	403 (49,642)	487 (03.84)	84	411.50	0.912	H→L (92%)	2.11	532	9.24	0.012
Acetone	403 (69,443)	488 (04.02)	85	412.32	0.881	H→L (90%)	2.31	–	–	0.01
EtOH	409 (45,206)	509 (03.39)	100	412.32	0.882	H→L (90%)	0.81	–	–	0.009
MeOH	403 (42,917)	502 (03.22)	99	412.46	0.864	H→L (90%)	2.35	543	8.17	0.006
ACN	400 (45,579)	491 (03.50)	91	412.46	0.873	H→L (90%)	3.11	–	–	0.006
DMF	409 (45,252)	501 (05.05)	92	412.46	0.921	H→L (90%)	0.84	531	5.98	0.008

[a] Experimental absorption wavelength

[b] Experimental emission wavelength

[c] Computed absorption wavelength

[d] Oscillator strength

[e] % Deviation between experimental absorption and vertical excitation computed by DFT

[f] % Deviation between experimental emission and computed (TD-DFT) emission

[Φ] Quantum yield at various solvents

– Not calculated

Table 9 Observed UV-Visible absorption-emission and its computed vertical excitation spectra of absorption-emission of dye 8f in different solvents

Solvents	Experimental			Computed (TD-DFT)						Φ
	λ_{max}[a] nm ( )	λ_{max}[b] nm intensity (au)	Stokes shift	Vertical[c] excitation (nm)	f[d]	Orbital contribution	%D[e]	TD-DFT emission (nm)	%D[f]	
THF	388 (36,443)	476 (22.71)	88	400.35	1.366	H→L (90%)	3.18	–	–	0.11
EtOAc	385 (34,232)	533 (23.16)	148	400.98	1.355	H→L (90%)	4.15	–	–	0.10
DCM	388 (29,504)	501 (05.51)	113	401.89	1.372	H→L (90%)	3.58	505	0.80	0.03
Acetone	388 (38,756)	483 (14.38)	95	403.07	1.341	H→L (90%)	3.88	–	–	0.07
EtOH	394 (45,746)	488 (10.05)	94	403.33	1.341	H→L (90%)	2.37	–	–	0.06
MeOH	382 (28,270)	480 (09.74)	98	403.46	1.326	H→L (90%)	5.62	517	7.71	0.05
ACN	382 (42,765)	486 (08.34)	104	403.46	1.333	H→L (90%)	5.62	–	–	0.05
DMF	385 (47,237)	489 (06.72)	104	403.59	1.370	H→L (90%)	4.83	518	5.93	0.04

[a] Experimental absorption wavelength

[b] Experimental emission wavelength

[c] Computed absorption wavelength

[d] Oscillator strength

[e] % Deviation between experimental absorption and vertical excitation computed by DFT

[f] % Deviation between experimental emission and computed (TD-DFT) emission

[Φ] Quantum yield at various solvents

–Not calculated

transition energy difference between HOMO and LUMO is 3.013 eV (411 nm), 3.085 eV (401 nm) in DCM respectively. There is a significant difference (~8 nm), (~12 nm) between the experimental absorption and the computed vertical excitation, and the % deviation is between 0.81–3.11 % and 2.37–5.62 % in the solvents studied respectively. The intense fluorescence emission peaks are observed in THF and DCM compared to methanol, ethanol, DMF, DMSO. The largest difference between the experimental emission and the computed emission wavelength are 45 nm in DCM and 37 nm in methanol respectively (Tables 8 and 9).

Frontier Molecular Orbitals

The different frontier molecular orbitals were studied to understand the electronic transition and charge delocalization within these styryl push-pull chromophores. The comparative increase and decrease in the energy of the highest occupied molecular orbital (HOMO's) and lowest unoccupied molecular orbitals (LUMO's) gives a qualitative idea of the excitation properties. The first allowed and the strongest transitions of electron with principal oscillator strength usually correspond almost exclusively to the transfer of an electron from HOMO-

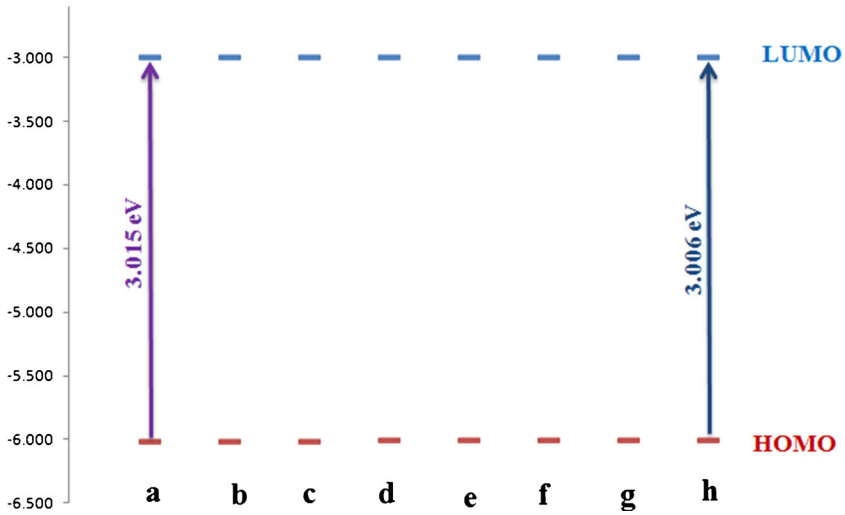

Fig. 5 Energy gap between HOMO → LUMO of the dye **8e** in Different solvents. Where, a = Tetrahydrofuran, b = Ethyl acetate, c = Acetone, d = Dichloromethane, e = Ethanol f = Methanol, g = Acetonitrile, h = N,N-Dimethylformamide

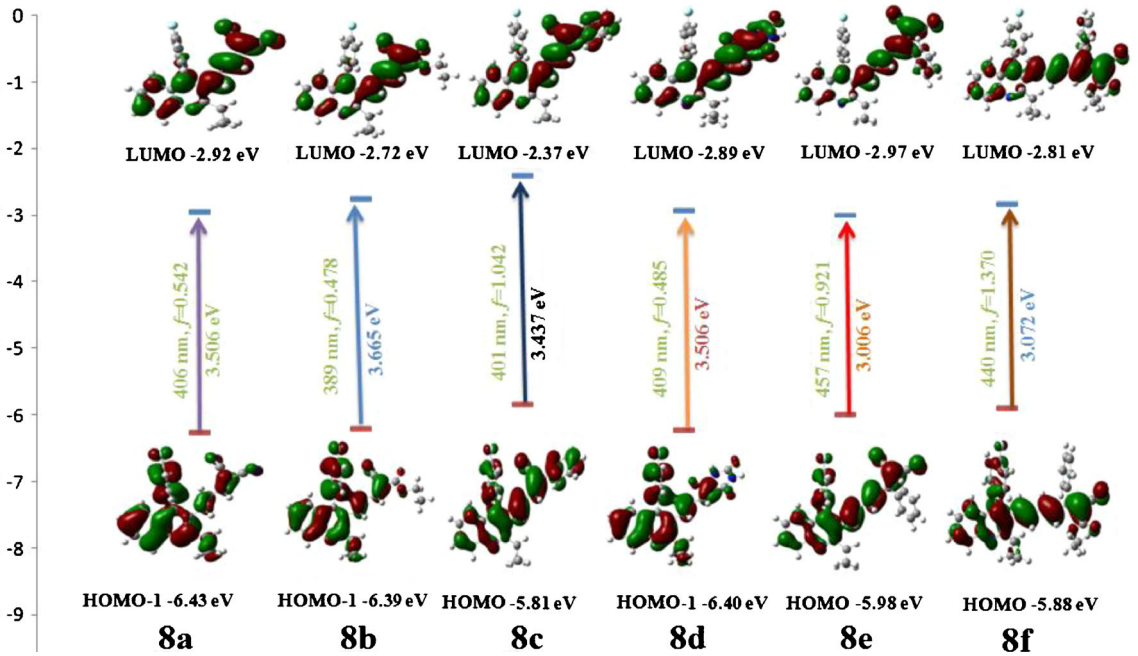

Fig. 6 Frontier molecular orbitals of dyes **8a–8f** in the ground state in DCM

1 → LUMO for the dyes 8a, 8b, 8d and HOMO → LUMO for the dyes 8c, 8e, 8 f. Tables S1-S6 show the energies of the different molecular orbitals in different solvents involved in the electronic transitions of these push-pull styryl dyes. In the case of all the synthesized styryl dyes the energy gap of HOMO-1 → LUMO and HOMO → LUMO orbitals remained irrespective of the solvent polarity, either increased or decreased (Fig. 5, Tables S1-S6). The LUMO energy level of the compounds 8a and 8e are −2.94, −2.98 eV, similarly for the dyes 8b and 8f are −2.72, −2.80 eV, and in DCM the value remained same. It may be due to the very similar reduction potential (Fig. 6). This is understandable because of the

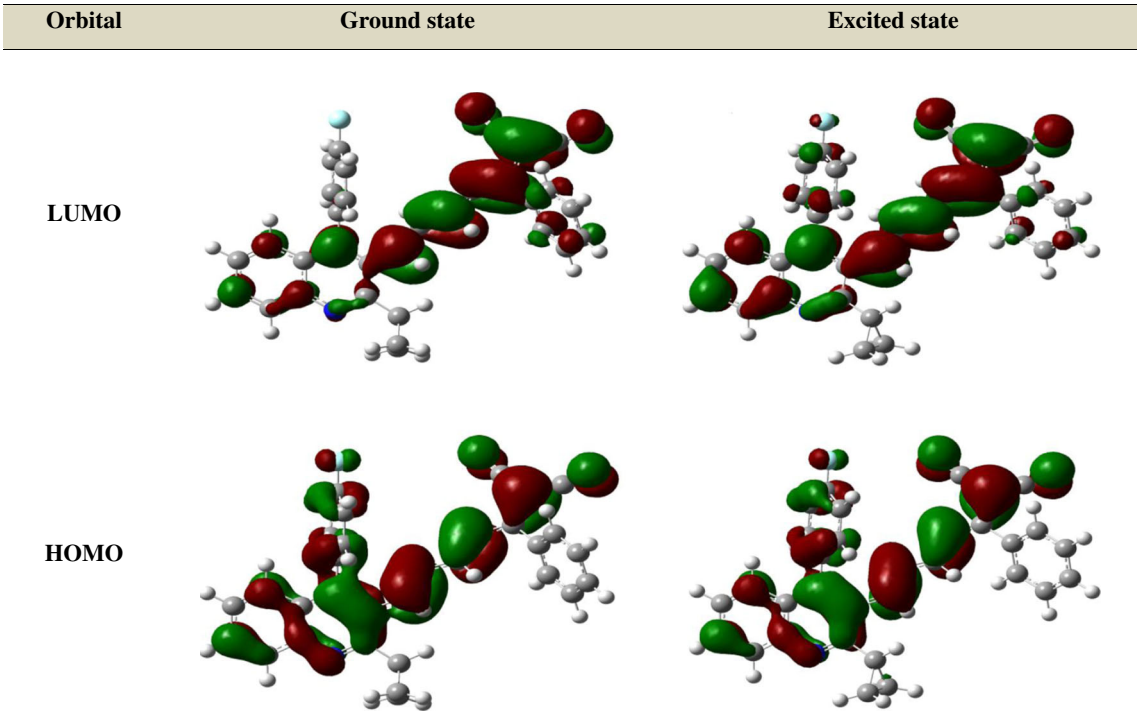

Fig. 7 Frontier molecular orbitals of dye **8e** in the ground and excited state in DCM

Table 10 Static first hyperpolarizability and its β -components of dyes 8a-8f (all values in e.s.u.)

β-tensors	8a	8b	8c	8d	8e	8f
β_{xxx}	-3.40×10^{-29}	-4.4×10^{-29}	-1.22×10^{-29}	-4.8×10^{-29}	9.37×10^{-29}	-6.77×10^{-29}
β_{xxy}	1.26×10^{-29}	-2×10^{-31}	-1.33×10^{-30}	1.11×10^{-29}	4.82×10^{-30}	1.33×10^{-29}
β_{xyy}	-4.5×10^{-30}	1.41×10^{-30}	1.6×10^{-30}	-2.2×10^{-30}	-3.88×10^{-30}	-2.25×10^{-30}
β_{yyy}	-4.4×10^{-31}	-1.3×10^{-30}	-1.75×10^{-30}	-1.7×10^{-30}	2.52×10^{-30}	-5.7×10^{-30}
β_{xxz}	1.11×10^{-31}	-1.8×10^{-30}	-1.53×10^{-30}	3.15×10^{-30}	-3.71×10^{-30}	-4.88×10^{-31}
β_{yyz}	-1.7×10^{-31}	1.98×10^{-31}	-2.62×10^{-31}	-8.8×10^{-31}	1.44×10^{-30}	-8.67×10^{-31}
β_{xzz}	-4.9×10^{-31}	-4.2×10^{-31}	-4.2×10^{-31}	-8.6×10^{-31}	-1.13×10^{-30}	-1.55×10^{-30}
β_{yzz}	1.99×10^{-32}	-1.7×10^{-31}	-5.85×10^{-31}	-4.4×10^{-31}	-4.29×10^{-31}	-3.79×10^{-32}
β_{zzz}	2.33×10^{-31}	2.86×10^{-31}	2.68×10^{-31}	1.47×10^{-32}	-1.12×10^{-31}	-1.12×10^{-30}
β_o	400.09×10^{-31}	425.44×10^{-31}	116.61×10^{-31}	518.42×10^{-31}	898.48×10^{-31}	702.72 10–31

reduction site, the dye 8a, 8e and 8b, 8f assuming the dicyano and cyano, carbethoxy in the same chemical structure of dyes [45].

The molecular orbital diagram (isodensity plots) for the dyes 8a, 8e and 8b, 8c 8d, 8f are shown in Fig. 6. From the pictorial diagram of the dyes 8a and 8e it was found that HOMO-1 → LUMO and HOMO → LUMO orbitals are fully delocalized on the donor 4-fluorophenyl ring along with the quinoline moiety and the acceptor cyano group through the π-bond conjugation respectively. The electron densities in the HOMOs of all the dyes were largely located on the donor 4-(4-fluorophenyl)quinoline moiety, and the electron densities on the LUMOs were found localized on the acceptor through the π-bridge. The excitation from HOMO to LUMO mostly consists of the charge transfer from the 4-fluorophenyl) and the quinoline moiety to the acceptor end. The energy gap of HOMO-1 or HOMO / LUMO explains the charge transfer interactions and the non-linear properties of the dyes. Figure 7 contains FMO of the dye 8e in the excited state, which shows that the electron densities are located on the donor 4-fluorophenyl and the quinoline moiety in the HOMO and these electron densities were fully transferred on the acceptor moiety in the LUMO.

Static Second-order Nonlinear Optical (NLO) Properties

The D-π-A chromophores are expected to have good non-linear properties and their first hyperpolarizability (β_o) values can be enhanced due to their relative orientation. Thus, their good linear and nonlinear optical properties of the asymmetrical push-pull chromophores have been studied. Density functional theory (DFT) was used to calculate the second-order NLO properties of the quinoline styryl D-π-A chromophores. The static first hyperpolarizability (β_o) and its related properties for the dyes 8a-8f were calculated using B3LYP/6-31G(d) on the basis of the finite field approach [46]. The computed first hyperpolarizability (β_o) values were found to be ranging from 400.09, 425.44, 116.61, 518.42, 898.48, 702.72×10^{-31} e.s.u. for the dyes 8a, 8b, 8c, 8d, 8e and 8f respectively. The computed β-tensors are summarized in Table 10. These values are greater than the values for urea (3.8×10^{-31} e.s.u.) by 105, 112, 30, 136, 235 and 184 times respectively. These dyes have shown a large hyperpolarizability, significantly considerable charge transfer characteristics of the ground state to the first excited state. This is further supported by the large variation in the dipole moments between the ground and the excited states from the solvatochromism studies. From these observations it was clear that, these dyes could be used as promising candidates in the field of non-linear optics.

Thermal Stability

The dye molecules should form compact aggregates due to the strong intermolecular interactions so that they can acquire high thermal stability [47]. In order to assess the thermal properties of the dyes, thermal stability studies have been carried out using thermal gravimetric techniques (TGA) in the temperature range 40–600 °C under nitrogen gas at a

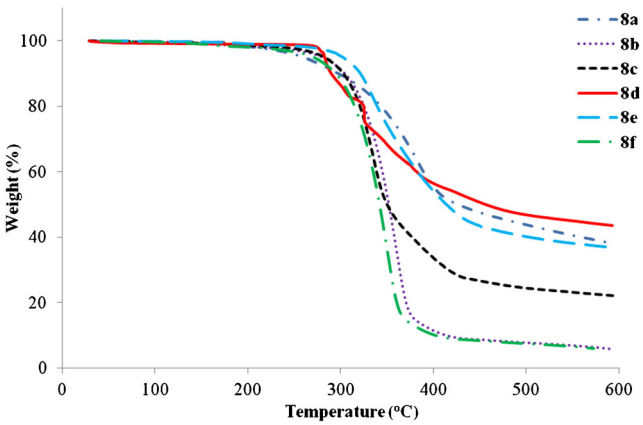

Fig. 8 Thermogravimetric analysis overlay graph of dyes **8a–8f**

heating rate of 10 °C min^{-1}. The TGA results indicated that the synthesized styryl dyes are stable up to 250 °C. TGA revealed the onset decomposition temperature (Td) of dyes 8a, 8b, 8c, 8d, 8e and 8f are 254 °C (95 %), 262 °C (96 %), 273 °C (96 %), 275 °C (97 %), 287 °C (96 %), and 267 °C (95 %) respectively. In general the backbones of these styryl dyes are stable up to 250 °C and above 250 °C the thermo-gravimetric curve of these dyes showed a major loss in weight. The comparisons of the Td (decomposition temperature) show that the thermal stability of the styryl dyes decreases in the order 8a > 8b > 8f > 8c > 8d > 8e. The TGA results showed that the styryl dyes have good thermal stability. The dyes 8b, 8c and 8f showed a sharp decomposition after a temperature of 262 °C and 273 °C and 267 °C respectively and they completely decomposed beyond 500 °C. However, the dyes 8a, 8d and 8e showed sluggish decomposition nature and completely decomposed beyond 600 °C. The observations are summarized in Fig. 8.

Conclusion

In summary, we have designed and synthesized the novel D-π-A type chromophores containing the 4-fluorophenyl unit along with the quinoline ring as an electron donor and cyano/carbethoxy moieties as the electron acceptors. The structures of the synthesized styryl dyes were confirmed by FT-IR, ^1H NMR and Mass spectral analysis. The resultant photophysical data revealed that these dyes have a high Stokes shift ranging from 3,817 to 7,917 cm^{-1}. Also, their large dipole moments in the first excited state than in the ground state suggest a distinct charge delocalization in the first excited state. The significant emissive property implies that the electronic coupling between the donor and the acceptor was sufficient to allow a charge transfer within the molecule and they are sensitive towards the solvent polarity. The quantum yield was observed to be comparatively higher in non-polar solvent than polar solvent. The synthesized styryl dyes have good thermal stability.

The geometry of the styryl dyes were optimized at B3LYP/6-31G(d) level. The vertical excitations and emissions were computed and are in good agreement with the experimental results. The dyes 8a, 8b, 8d and 8c, 8e 8f have shown a prominent absorption at the longer wavelength due to HOMO→LUMO and HOMO-1→LUMO transition with a high oscillator strength respectively. The isodensity orbital plots have displayed that majority of the electron density is located on the chromophores 4-(4-fluorophenyl)quinoline. The first hyperpolarizability was calculated by using the finite field approach at B3LYP/6-31G(d) level and it was found that these dyes possess a large second-order nonlinear property. This is attributed to the excited state intramolecular charge transfer mainly due to the strong donor-π-acceptor conjugation.

Thus here we describe the synthesis, characterization, photo-physical and thermal properties along with DFT study of these twisted donor-π-acceptor quinoxaline styryl dyes. These styryl dyes could be used as promising candidates for various applications in nonlinear optics (NLO), electronic-photonic devices and organic light emitting diodes.

Acknowledgments The authors are greatly thankful to TIFR, SAIF-I.I.T. Mumbai for recording the ^1H-NMR and Mass spectra. One of the authors Mininath S. Deshmukh is grateful to CSIR for financial support.

References

1. Fox MA (1992) Introduction - electron transfer: a critical link between subdisciplines in chemistry. Chem Rev 92:365–368. doi:10.1021/cr00011a600
2. Lakowicz JR (1994) Probe design and chemical sensing topics in fluorescence spectroscopy, 4th edn. 501–504
3. Balaganesan B, Wen S-W, Chen CH (2003) Synthetic study of tetramethyljulolidine—a key intermediate toward the synthesis of the red dopant DCJTB for OLED applications. Tetrahedron Lett 44:145–147. doi:10.1016/S0040-4039(02)02506-6
4. Yu G, Gao J, Hummelen JC et al (1995) Polymer photovoltaic cells: enhanced efficiencies via a network of internal donor-acceptor heterojunctions. Science 270:1789–1791. doi:10.1126/science.270.5243.1789
5. Gold H (1971) The chemistry of synthetic compounds, fluorescent brightening agents. Venkataraman K 535–679
6. Shirota Y (2000) Organic materials for electronic and optoelectronic devices. J Mater Chem 10:1–25. doi:10.1039/A908130E
7. Sonawane YA, Phadtare SB, Borse BN et al (2010) Synthesis of diphenylamine-based novel fluorescent styryl colorants by knoevenagel condensation using a conventional method, biocatalyst, and deep eutectic solvent. Org Lett 12:1456–1459. doi:10.1021/ol902976u
8. Gupta VD, Padalkar VS, Phatangare KR et al (2011) The synthesis and photo-physical properties of extended styryl fluorescent derivatives of N-ethyl carbazole. Dye Pigment 88:378–384. doi:10.1016/j.dyepig.2010.08.013
9. Hranjec M, Kralj M, Piantanida I et al (2007) Novel cyano- and amidino-substituted derivatives of styryl-2-benzimidazoles and benzimidazo[1,2-a]quinolines. Synthesis, photochemical synthesis, DNA binding, and antitumor evaluation, part 3. J Med Chem 50:5696–5711. doi:10.1021/jm070876h
10. Zhang N, Zhao Y-Z, Zhang H-S, Wang H (2008) Sensitive determination of aliphatic amines by high-performance liquid chromatography with a new fluorogenic probe 3-(4-fluorinebenzoyl)-2-quinoline carboxaldehyde. J Sep Sci 31:38–46. doi:10.1002/jssc.200700341
11. Shiraishi Y, Ichimura C, Hirai T (2007) A quinoline–polyamine conjugate as a fluorescent chemosensor for quantitative detection of Zn(II) in water. Tetrahedron Lett 48:7769–7773. doi:10.1016/j.tetlet.2007.09.032
12. Perin N, Hranjec M, Pavlović G, Karminski-Zamola G (2011) Novel aminated benzimidazo[1,2-a]quinolines as potential fluorescent probes for DNA detection: microwave-assisted synthesis, spectroscopic characterization and crystal structure determination. Dye Pigment 91:79–88. doi:10.1016/j.dyepig.2011.02.003
13. Ohshima R, Kitamura M, Morita A et al (2009) Design and synthesis of a fluorescent probe for Zn2+, 5,7-Bis(N, N-dimethylaminosulfonyl)-8-hydroxyquinoline-pendant 1,4,7,10-tetraazacyclododecane and Zn2+–dependent hydrolytic and Zn2+–independent photochemical

reactivation of its benzenesulfonyl-caged D. Inorg Chem 49:888–899. doi:10.1021/ic901279t
14. Ou S, Lin Z, Duan C, et al. (2006) A sugar-quinoline fluorescent chemosensor for selective detection of Hg2+ ion in natural water. Chem Commun 4392–4394. doi: 10.1039/B607287A
15. Mitscher LA (2005) Bacterial topoisomerase inhibitors: quinolone and pyridone antibacterial agents. Chem Rev 105:559–592. doi:10.1021/cr030101q
16. Wang Z, Vince R (2008) Synthesis of pyrimidine and quinolone conjugates as a scaffold for dual inhibitors of HIV reverse transcriptase and integrase. Bioorg Med Chem Lett 18:1293–1296
17. Bhanot SK, Singh M, Chatterjee NR (2001) The chemical and biological aspects of fluoroquinolones reality and dreams. Curr Pharm Des 7:331–335. doi:10.2174/1381612013398059
18. Baba Y, Saha G, Nakao S et al (2000) Asymmetric total synthesis of halicholactone. J Org Chem 66:81–88. doi:10.1021/jo001036c
19. Boger DL, Hughes TV, Hedrick MP (2001) Synthesis, chemical properties, and biological evaluation of CC-1065 and duocarmycin analogues incorporating the 5-methoxycarbonyl-1,2,9,9a-tetrahydrocyclopropa[c]benz[e]indol-4-one alkylation subunit. J Org Chem 66:2207–2216. doi:10.1021/jo001772g
20. Graham DW, Ashton WT, Barash L et al (1987) Inhibition of the mammalian.beta.-lactamase renal dipeptidase (dehydropeptidase-I) by Z-2-(acylamino)-3-substituted-propenoic acids. J Med Chem 30:1074–1090. doi:10.1021/jm00389a018
21. Tsuji T, Nishida S (1987) The chemistry of the cyclopropyl group. Wiley and sons, New York
22. Rappoport Z (1996) The chemistry of the cyclopropyl group. Wiley, New York
23. Salaün J (2000) Cyclopropane derivatives and their diverse biological activities. In: Meijere A (ed) Small ring compd. Org. Synth. VI SE - 1. Springer, Berlin
24. Ellis D, Kuhen KL, Anaclerio B et al (2006) Design, synthesis, and biological evaluations of novel quinolones as HIV-1 non-nucleoside reverse transcriptase inhibitors. Bioorg Med Chem Lett 16:4246–4251. doi:10.1016/j.bmcl.2006.05.073
25. Fu H, Wu H, Hou X et al (2006) N-Aryl carbazole derivatives for non-doped red OLEDs. Synth Met 156:809–814. doi:10.1016/j.synthmet.2006.04.013
26. Zhu W, Meng X, Yang Y et al (2010) Bisthienylethenes containing a benzothiadiazole unit as a bridge: photochromic performance dependence on substitution position. Chem Eur J 16:899–906. doi:10.1002/chem.200901855
27. Xia Z-Y, Zhang Z-Y, Su J-H et al (2010) Robust and highly efficient blue light-emitting hosts based on indene-substituted anthracene. J Mater Chem 20:3768–3774. doi:10.1039/C000092B
28. Tan Y, Yu J, Gao J et al (2013) A new fluorescent and colorimetric probe for trace hydrazine with a wide detection range in aqueous solution. Dye Pigment 99:966–971. doi:10.1016/j.dyepig.2013.08.008
29. Jamorski Jödicke C, Lüthi HP (2003) Time-dependent density functional theory (TDDFT) study of the excited charge-transfer state formation of a series of aromatic donor-acceptor systems. J Am Chem Soc 125:252–264. doi:10.1021/ja020361+
30. Gupta VD, Tathe AB, Padalkar VS et al (2013) Red emitting solid state fluorescent triphenylamine dyes: synthesis, photo-physical property and DFT study. Dye Pigment 97:429–439. doi:10.1016/j.dyepig.2012.12.024
31. Brouwer AM (2011) Standards for photoluminescence quantum yield measurements in solution (IUPAC Technical Report). Pure Appl Chem 83:2213–2228. doi:10.1351/PAC-REP-10-09-31
32. Frisch MJ, Trucks GW, Schlegel HB, et al. (2009) Gaussian 09 C.01
33. Treutler O, Ahlrichs R (1995) Efficient molecular numerical integration schemes. J Chem Phys 102:346
34. Becke A (1993) A new mixing of Hartree-Fock and local density functional theories. J Chem Phys 98:1372
35. Lee C, Yang W, Parr RG (1988) Development of the Colle-Salvetti correlation-energy formula into a functional of the electron density. Phys Rev B 37:785–789
36. Valeur B (2001) Molecular fluorescence: principles and applications. Wiley, Weinheim
37. Lakowicz JR (1999) Principles of fluorescence spectroscopy, 2nd edn. Kluwer, New York
38. Cossi M, Barone V, Cammi R, Tomasi J (1996) Ab initio study of solvated molecules: a new implementation of the polarizable continuum model. Chem Phys Lett 255:327–335. doi:10.1016/0009-2614(96)00349-1
39. Tomasi J, Mennucci B, Cammi R (2005) Quantum mechanical continuum solvation models. Chem Rev 105:2999–3094. doi:10.1021/cr9904009
40. Williams ATR, Winfield SA, Miller JN (1983) Relative fluorescence quantum yields using a computer-controlled luminescence spectrometer. Analyst 108:1067–1071. doi:10.1039/AN9830801067
41. Suzuki M, Iwasaki H, Fujikawa Y et al (2001) Synthesis and biological evaluations of quinoline-based HMG-CoA reductase inhibitors. Bioorg Med Chem 9:2727–2743. doi:10.1016/S0968-0896(01)00198-5
42. Suzuki M, Yanagawa Y, Iwasaki H et al (1999) First systematic chiral syntheses of two pairs of enantiomers with 3,5-dihydroxyheptenoic acid chain, associated with a potent synthetic statin NK-104. Bioorg Med Chem Lett 9:2977–2982. doi:10.1016/S0960-894X(99)00519-3
43. Strehmel B, Rettig W (1996) Photophysical properties of fluorescence probes I: dialkylamino stilbazolium dyes. J Biomed Opt 1:98–109. doi:10.1117/12.227538
44. Gromov SP, Ushakov EN, Fedorova OA et al (2003) Novel photoswitchable receptors: synthesis and cation-induced self-assembly into dimeric complexes leading to stereospecific [2+2]-photocycloaddition of styryl dyes containing a 15-crown-5 ether unit. J Org Chem 68:6115–6125. doi:10.1021/jo034460x
45. Chen C-T, Chiang C-L, Lin Y-C et al (2003) Ortho-Substituent effect on fluorescence and electroluminescence of arylamino-substituted coumarin and stilbene. Org Lett 5:1261–1264. doi:10.1021/ol034268h
46. Vidya S, Ravikumar C, Hubert Joe I et al (2011) Vibrational spectra and structural studies of nonlinear optical crystal ammonium D, L-tartrate: a density functional theoretical approach. J Raman Spectrosc 42:676–684. doi:10.1002/jrs.2743
47. Chunlong Z, Nianchun M, Liyun L (1993) An investigation of the thermal stability of some yellow and red azo pigments. Dye Pigment 23:13–23. doi:10.1016/0143-7208(93)80020-2